Title

Early behavioral and metabolomic change after mild to moderate traumatic brain injury in the developing brain.

Authors

Chitturi, Jyothsna
Li, Ying
Santhakumar, Vijayalakshmi
et al.

Publication Date

2018-11-01

DOI

10.1016/j.neuint.2018.08.003

Peer reviewed

HHS Public Access

Author manuscript

Neurochem Int. Author manuscript; available in PMC 2019 November 01.

Published in final edited form as:

Neurochem Int. 2018 November ; 120: 75–86. doi:10.1016/j.neuint.2018.08.003.

Early behavioral and metabolomic change after mild to moderate traumatic brain injury in the developing brain

Jyothsna Chitturi[1], **Ying Li**[2], **Vijayalakshmi Santhakumar**[2,3], and **Sridhar S. Kannurpatti**[*]

[1]Department of Radiology, Rutgers New Jersey Medical School, Administrative Complex Building 5 (ADMC5), 30 Bergen Street Room 575, Newark, NJ 07101, USA. Phone (Off): (973) 972-7417, Fax: (973) 972-7363, jc2248@njms.rutgers.edu

[2]Department of Pharmacology, Physiology & Neuroscience, Rutgers New Jersey Medical School, MSB-H-512, 185 S. Orange Ave, Newark, NJ 07103, USA. Phone (Off):(973) 972-2421, Fax:(973) 972-7950, yl691@njms.rutgers.edu

[3]Molecular, Cell and Systems Biology, University of California Riverside, Spieth 1308, 3401 Watkins Drive, Riverside, CA 92521, USA. Email: santhavi@njms.rutgers.edu

Abstract

Pathophysiology of developmental traumatic brain injury (TBI) is unique due to intrinsic differences in the developing brain. Energy metabolic studies of the brain during early development (P13 to P30) have indicated acute oxidative energy metabolic decreases below 24 hours after TBI, which generally recovered by 48 hours. However, marked neurodegeneration and altered neural functional connectivity have been observed at later stages into adolescence. As secondary neurodegeneration is most prominent during the first week after TBI in the rat model, we hypothesized that the subacute TBI-metabolome may contain predictive markers of neurodegeneration. Sham and TBI metabolomes were examined at 72 hours after a mild to moderate intensity TBI in male Sprague-Dawley rats aged P31. Sensorimotor behavior was assessed at 24, 48 and 72 hours after injury, followed by 72-hour postmortem brain removal for metabolomics using Liquid Chromatography/Mass Spectrometry (LCMS) measurement. Broad TBI-induced metabolomic shifts occurred with relatively higher intensity in the injury-lateralized (ipsilateral) hemisphere. Intensity of metabolomic perturbation correlated with the extent of sensorimotor behavioral deficit. N-acetyl-aspartate (NAA) levels at 72 hours after TBI, predicted the extent of neurodegeneration assessed histochemically 7-days post TBI. Results from the multivariate untargeted approach clearly distinguished metabolomic shifts induced by TBI. Several pathways including amino acid, fatty acid and energy metabolism continued to be affected at 72 hours after TBI, whose collective effects may determine the overall pathological response after TBI in early development including neurodegeneration.

[*]Correspondence: Sridhar S. Kannurpatti, PhD Department of Radiology, Rutgers Biomedical and Health Sciences, New Jersey Medical School, ADMC-5, Room 575, 30 Bergen Street, Newark, NJ 07101, USA. Tel:973-972-7417, kannursr@njms.rutgers.edu.

Author contributions.

SK conceived and designed the study, JC, YL and SK performed the experiments, JC analyzed data, VS contributed to significant laboratory resources and expertise for the animal model of Traumatic Brain Injury. JC and SK wrote the first draft of the manuscript and all authors read and approved the submitted version of the manuscript.

Conflict of interest.

The authors declare no conflicts related to the subject matter or materials discussed in the manuscript.

Keywords

traumatic brain injury; sensorimotor behavior; metabolomics; glycolysis; TCA cycle; mass spectrometry; liquid chromatography; pediatric; glycolysis; fluid percussion

1. Introduction

A majority of traumatic brain injuries (TBI) are in the mild to moderate range with children and adolescents forming a major share of the TBI cases worldwide (Faul et al., 2010). In order to understand the early stage TBI pathophysiology, acute/subacute brain biochemical pathways have been studied between 0–72 hours using preclinical animal models, which have consistently indicated energy metabolic stress (Casey et al., 2008; Marino et al., 2007; Pascual et al., 2007; Robertson et al., 2013; Robertson et al., 2006). Early-stage bioenergetic stress, combined with hyper excitability of neural populations, is hypothesized to contribute to excitotoxic secondary injury in the brain after a TBI. As the developing brain is biased towards excitatory neurotransmission (Mcdonald et al., 1988b), it is relatively more vulnerable to secondary excitotoxic injury (McDonald et al., 1988). Targeted metabolite studies of the developing brain indicate depressed oxidative metabolism up to 24 hours after TBI, which largely recovered by 48 hours (Robertson et al., 2013; Thomas et al., 2000). However, neurodegeneration continues throughout the acute/subacute window with maximum neuronal death occurring between 0–7 days after TBI in the preclinical rat model (Lifshitz and Lisembee, 2011). Thus characterizing the TBI metabolome beyond 48 hours and integrating it with behavioral and neurodegenerative outcomes can improve current understanding of the acute/subacute stage response to TBI sustained during early development.

Metabolomic studies provide comprehensive information on various *in vivo* enzymatic activities and have been successfully applied to obtain disease markers in neurodegenerative pathologies. TBI metabolomic marker characterization have been performed using Nuclear Magnetic Resonance (NMR) (Bahado-Singh, 2016b; Glenn et al., 2013; Robertson et al., 2013; Viant et al., 2005), or Mass Spectrometry (MS) of lipids (Emmerich et al., 2016; Emmerich et al., 2017; Sheth et al., 2015), targeting smaller and specific classes of metabolites or liquid chromatography/mass spectrometry (LCMS) based metabolomics, targeting broader biochemical changes (Bahado-Singh, 2016a; Daley, 2016; Oresic et al., 2016; Yi et al., 2016; Zheng et al., 2017). In order to target a wide range of metabolites in the developing brain, we performed LC-MS based brain tissue metabolomics in a preclinical rat model subjected to a fluid percussion TBI. As secondary neurodegeneration is most prominent during the early window of 0–7 days in the current preclinical rat model of TBI, we hypothesized that the subacute TBI-metabolome may provide predictive biomarkers of neurodegeneration. Sham and TBI metabolomes were analyzed at 72 hours after TBI, providing sufficient time for the recovery of energy metabolism, known to occur by 48–72 hours after injury (Robertson et al., 2013; Thomas et al., 2000). A total of 197 metabolites were identified and characterized from postmortem brain extracts, encompassing different classes of metabolites including amino acids, neurotransmitters, carbohydrates, small organic acids and ketone bodies.

2. Materials and Methods

2.1. Animals

Male Sprague-Dawley rats (~23 days old; weighing 60–70g) were procured from Charles River Laboratories, Wilmington, MA, USA. A total of 25 animals were housed under controlled conditions and used for the experiments at age 31 days. 24 animals survived and were used for the results and characterization. All procedures were approved by the Institutional Animal Care and Use Committee of Rutgers Biomedical and Health Sciences-New Jersey Medical School and conducted in accordance with the National Institutes of Health guide for the care and use of Laboratory animals (NIH Publications No. 8023, revised 1978). Experimental timeline of injury, metabolomic analysis, behavior and histology are shown in Figure 1A. Blinding of animal groups was not performed as the same personnel performing injury in the animal subjects performed the behavioral tests.

2.2. Lateral fluid-percussion injury

Animals (n=25) were randomly subjected to sham procedure or lateral fluid percussion injury (FPI) as previously described (Gupta et al., 2012; Murugan et al., 2016). The FPI procedure is known to produce diffuse TBI. In brief, the rats were anesthetized with Ketamine (80mg/kg i.p)-Xylazine (10mg/kg i.p) and positioned on a stereotaxic frame. A 3mm craniotomy was performed on the left side of the skull −5 mm posterior to the bregma and 3 mm lateral to the sagittal suture keeping the dura intact (surgeries were performed by a single surgeon to minimize inter-subject variability in the craniotomy procedure). A Luer-Lock syringe hub was glued surrounding the exposed dura using a cyanoacrylate adhesive. After a 24 hour recovery period, TBI was induced by attaching the Luer-Lock hub of an isoflurane-anesthetized rat to the FPI device (Virginia Commonwealth University, VA, USA). A pendulum drop delivered a brief 20ms impact on the intact dura. The impact pressure was measured by an extra-cranial transducer and controlled between 1.8–2.0 atm. For the sham group, animals underwent the same procedures as the injury group including attachment to the FPI device under isoflurane anesthesia, but without the pendulum drop. A total of 24surviving animals sham (n=10) and TBI animals (n=14) were monitored within their cage environment on a daily basis throughout the experimental time line. One TBI animal expired immediately within 30 minutes after the TBI procedure and was not considered for further data analysis. Rats were anesthetized using 2% isoflurane in an induction chamber and quickly transferred to the injury device. Overall duration of isoflurane anesthesia was approximately 2–3 minutes. After injury, rats were transferred to a soft bedding cage and monitored for the return of righting reflex and any signs of seizures for the next 30 minutes. No special temperature management was necessary.

2.3. Sample Preparation, tissue sample extraction and Liquid Chromatography/Mass Spectrometry (LC/MS)

72 hours after sham or TBI procedures, rats were euthanized by cervical dislocation, decapitated and the brains were rapidly dissected out. The cerebellum and brain stem were removed (not considered for the study) and the two cerebral hemispheres separated along with midline (containing both cortical and sub-cortical regions), placed into vials and frozen

immediately in liquid nitrogen. Brain tissue samples were stored at −80°C for metabolomic analysis.

Metabolite analysis by LC-MS was performed as described in previous studies (Yuan et al., 2012). Briefly, each sample was transferred to a pre-cooled (dry ice) homogenization tube and 4 ml of pre-cooled 80% methanol (extraction buffer) was added to each sample and homogenization was performed for 15 seconds using the standard micro homogenizer (Pro Scientific). 500μL of sample was taken out to a new Eppendorf tube and centrifuged at 4°C at 14,000 rpm for 15 minutes. Supernatant was collected and lyophilized to pellet with no heat. All samples were normalized to tissue weight.

Targeted LC/MS analyses were performed on the brain extract samples using a Q ExactiveOrbitrap mass spectrometer (Thermo Scientific) coupled to a Vanquish UPLC system (Thermo Scientific). The Q Exactive operated in a polarity-switching mode. A Sequent ZIC-HILIC column (2.1 mm i.d. × 150mm; Merck. Co, USA), was used for separation of metabolites. Buffers consisted of HPLC bufferA (100% acetonitrile), and HPLC buffer B (pH=9.0: 95% (vol/vol) water, 5% (vol/vol) acetonitrile, 20mM ammonium hydroxide, 20 mM ammonium acetate). HPLC flow rate was set at 150 μL/min and gradients were from 85% to 30% for buffer A in 20 min followed by a wash with 30% buffer A and reequilibration at 85% buffer A. Metabolites were identified on the basis of exact mass within 5 ppm and standard retention times. Relative metabolite quantification was performed based on peak area for each of the identified metabolite.

2.4. Metabolite Data analysis and statistics

Statistical comparisons between hemispheres of sham and TBI were made as shown in Figure 1B. Data analysis was performed using the software Metaboanalyst 3.0 (http://www.metaboanalyst.ca) (Xia et al., 2009; Xia et al., 2015). To minimize variations introduced during sample preparation effects of ion suppression, metabolite peak intensities were normalized to tissue wet-weight. Data displayed equal variances as tested by the Levene's test but deviated from normality as tested by Shapiro-Wilk's test. Hence data were transformed to log base 10 to make the distribution normal and further auto-scaled (mean-centered and divided by the standard deviation of each variable). Hence the data after scaling were effectively the Z-scores. Plots of fold change in log scale were determined to efficiently represent metabolite concentration changes in both directions (increase or decrease). Volcano plots of significantly changing metabolites were determined using a two-sample Student's *t*-test with a probability threshold of $P<0.05$ corrected for multiple comparisons using the false discovery rate (FDR) for type-1 error control.

Subsequently multivariate approaches considering several dependent variables were used in order to determine changes at the metabolome level between sham and TBI animals. Partial least squares discriminant analysis (PLS-DA) was used to determine the separation between groups of the metabolite variables through rotation of the principal components. This multivariate analysis was used due to the presence of more metabolite variables than observations in addition to correlation among the variables the data (Tang et al., 2014). PLS-DA 2D and 3D score plots were generated from the first two and first three principal components respectively for classification. The PLS-DA analysis was also used for feature

selection and feature importance measures were generated (VIP: Variable Importance in Projection). R^2X and R^2Y, the fraction of variation that the model explains in the independent variables (X) and dependent variables (Y) and Q^2Y, the predictive accuracy of the model were estimated by the PLS-DA cross validation. These variables range between 0–1 with values >0.5 indicating good and >0.8 indicating outstanding predictive accuracies respectively. Loading plots (top 25 variables) were used to determine the clustering of variables and whether their relationship within (weightings) scores changed in response to TBI.

Hierarchical clustering method (HCM), a supervised pattern recognition method within Metaboanalyst 3.0, was used along with Pearson's correlation coefficient as a measure of similarity between metabolites. Correlation matrix of all metabolites, correlation matrix of samples and heat map of all variables were generated. The heat map plot using a statistical threshold of 25 best hits based on two-sample t-test were considered for the results and further analysis.

To measure the impact of individual metabolite changes on biochemical pathways, metabolic pathway analysis (MetPA) (Xia and Wishart, 2010a), and metabolite set enrichment analysis (MSEA) (Xia and Wishart, 2010b) were performed. MetPA combined results from pathway enrichment analysis with pathway topology analysis using a high-quality KEGG metabolic pathway database. Data were analyzed using a pre-existing rat reference library along with the global test algorithm for MSEA and relative-between centrality algorithm for pathway topology analysis provided within the Metaboanalyst software. Pathway enrichment analysis used metabolite concentration values to calculate p-values based on the asymptotic distribution without using permutations. Since many pathways were tested simultaneously, p-values were corrected for multiple comparisons using Holm-Bonferroni method (Holm P) and false discovery rate (FDR). Pathway topology analysis estimated node importance based on two node centrality measures, namely, degree centrality and betweenness centrality. While degree centrality represented the number of links converging on a node, betweenness centrality represented the number of shortest paths passing through the node. Different from the degree centrality measure focusing on local connectivity, the betweenness centrality measure focused on global network topology. Hence our analysis used betweenness centrality measure to calculate the pathway impact values (Impact) in MetPA.

MSEA directly investigates a set of functionally related metabolites without the need to preselect metabolites based on some arbitrary cut-off threshold and identifies biologically meaningful patterns that are significantly enriched (Xia and Wishart, 2010b). It has the potential to identify subtle but consistent changes among a group of related compounds in a certain biological pathway. A quantitative Enrichment Analysis (QEA) algorithm and a custom-made metabolite set library containing 36 metabolite sets based on metabolic pathways related to the detected brain metabolites was used as the reference library. The enrichment analyses considered reference metabolome built based on our analytical platform of the 196 targeted brain metabolites. A global test algorithm using a generalized linear model was used to estimate a Q-statistic for each metabolite set describing the correlation between metabolite concentration profiles (X) and physiological outcomes (Y). Q statistic

for each metabolite was derived from the average of the Q statistics for each metabolite within the set. Statistical p-values after MSEA were corrected for multiple comparisons using the Holm-Bonferroni method (Holm P) and False Discovery Rate (FDR).

2.5. Whisker Stimulation-Induced Motor Response (WSIMR)

To assess early sensorimotor defects, whisker stimulation-induced motor response (WSIMR) was performed 24, 48, and 72 hrs after injury. The WSIMR test is an adaptation of previously established whisker stimulation induced paw placement test in adult animals (Schallert et al., 2000). We have successfully modified this sensorimotor test to developmental stage animals as established by our previous studies (Murugan et al., 2016). Animals were placed in a test cage and left to habituate for 1min. Subsequently, whiskers on either side were stroked in a rostro-caudal direction using an applicator stick. Each trial consisted of multiple strokes at 3 Hz frequency and up to 10 trials were performed on each side of the animal with an inter-trial gap of 1 min. Responses were scored on a scale of 0–5. Active avoidance by running away with 1–2 strokes = 5; with 1–2 strokes, quick head movement away from the stroking stick = 4; slower head movement after 1–2 strokes away from the stick =3; head movement away from the stick after 3–6 strokes = 2; slower head movement after 3–6 strokes =1 and no reaction to stroking beyond 9 strokes = 0. An average score of the 10 trials was determined.

2.6. Forelimb Usage Test

Neural basis of spatial and motor behaviors, used as an assay of brain function, can be assessed by natural exploratory behavior in the rat. Forelimb usage test was a modified version of the cylinder test and provides a way to evaluate spontaneous forelimb usage in the home cage environment. Using this test, each animal was observed for 5 minutes duration in a test cage 24, 48, and 72 hrs after injury. Active exploration of vertical surfaces by rearing up on their hind limbs and wall surface exploration with their forelimbs were observed and scored. Number of independent wall placements observed for either one forelimb or both forelimbs was scored on a scale of 0–6. Animals using both forelimbs simultaneously, reaching to the top of the cage with more time exploring the cage wall=5; usage of both forelimbs, reaching the middle of the cage=4; exploring cage wall with only one forelimb usage=3; only one forelimb on the cage wall with little stability of the limb =2; only one forelimb on the surface and unable to lean on the cage wall=1. An average score of the activity within the 5 minutes observation duration was determined.

Forelimb usage test was further modified to evaluate spontaneous usage of contralateral and ipsilateral forelimbs more accurately. Number of independent wall placements observed for contralateral, ipsilateral, or both forelimbs were scored. Animals using both forelimbs simultaneously-5; exploring cage wall with only contralateral forelimb usage=4; exploring cage wall with only ipsilateral forelimb usage=3. Percentage forelimb usage within the 5 minutes observation duration was determined. Percentage forelimb usage was further normalized to sham to see percentage increase or decrease in TBI animals.

2.7. Histology

Postmortem animals were perfused with 4% paraformaldehyde in PBS, pH 7.4 and brains were removed and post-fixed in the same paraformaldehyde solution for 24 hours. Following post-fixation, brains were cryoprotected in 30% sucrose in PBS for 48 hrs. Coronal sections (40μm-thickness) were cut using a Leica cryostat at −0.1 mm with respect to the Bregma encompassing the sensorimotor cortex and sufficiently distant from the injury site. Sections were mounted on gelatin-coated glass and stained with Cresyl violet to mark the neurons. Brain tissue sections from both the injured-ipsilateral hemisphere and the uninjured-contralateral hemisphere were used for histological evaluations. To assess neuronal cell survival, six random counting frames per animal (three in each hemisphere) were placed covering all layers of the whisker barrel cortex ($S1_{BF}$). Nissl bodies of neuronal cytoplasm were manually counted within each field of view using a magnification of 40x using an oil immersion objective on an inverted optical microscope.

3. Results

Subacute stage brain metabolic changes 72 hours after TBI or sham injury were determined using LC-MS. A total of 197 metabolites were characterized including amino acids, neurotransmitters, carbohydrates, small organic acids, and ketone bodies. As the TBI was lateralized, metabolite differences were compared both within group (between hemispheres) and across sham and TBI groups (corresponding hemispheres) (Figure 1B) and integrated with behavioral outcomes. Histological outcomes were compared with N-acetyl aspartate (NAA) concentration, a neuronal specific metabolite and robust marker for neuronal viability (Demougeot et al., 2001; Tallan et al., 1956).

3.1. Effect of craniotomy and luer-lock implantation on the metabolite profile

Initially we compared between ipsilateral and contralateral hemispheres of sham animals to verify if craniotomy procedure (required for the FPI) itself caused any metabolomic perturbation. Figure 2A shows the metabolite fold change (FC) in logarithmic scale and Figure 2B, **shows the univariate analysis volcano plots with significantly changed metabolites above the multiple comparison corrected threshold of P<0.05 after a two-sample student's t-test. The craniotomy procedure itself induced a significant change in about ~2.5% of the targeted metabolites (Figure 2B)**. Multivariate analyses using PLS-DA (Figure 2C,D) confirmed a partial class separation with a positive accuracy value of the PLS-DA model (Accuracy=0.66, R^2 value=0.98, Q^2 value=0.26) (Figure S1B).To ascertain the nature of metabolomic shift after craniotomy, a hierarchical clustering (using Pearson's correlation coefficient) was used to generate the correlation map of all metabolites between the ipsilateral and contralateral hemispheres in sham animals. Correlation matrix using a statistical threshold of 25 best hits based on two-sample t-test showed changes in mostly amino acids/neurotransmitters and certain energy related metabolites **(**Figure S1A**)**.

Metabolites coupled via their relationship to biochemical pathways may show correlated changes and less likely to represent as false positives/negatives when considered as a cluster. Hence we performed MetPA and MSEA, providing information on significant and biochemical pathway-based coordinated changes in metabolites. Pathway analysis

comparison between sham ipsilateral and contralateral hemispheres showed significant changes (Holm P<0.05) in primary bile acid biosynthesis, pyruvate, glyoxylate and dicarboxylate metabolism (Figure 2E). **Further analysis using MSEA showed significant fold enrichment (Holm P<0.05) in metabolite clusters related to nicotinate and nicotinamide metabolism, glutamate, glycine, serine and tryptophan metabolism, malate-aspartate shuttle and glycolysis (Figure 2F)**.

3.2. Bilateral brain metabolomic alterations after TBI

Within TBI animals, ipsilateral and contralateral brain hemispheres showed metabolite differences with ~13% of the metabolites showing a two-fold change (Figure 3A). As observed by the volcano plots, 2.5 % of them showed significant differences (Figure 3B). Multivariate analyses using PLS-DA (Figure 3C, D) showed a partial class separation with a positive accuracy value of the PLS-DA model (Accuracy=0.91, R^2 value=0.91, Q^2 value=0.62) (Figure S2B). Hierarchical clustering showed changes in amino acids/ neurotransmitters, TCA cycle components between hemispheres after TBI (Figure S2A) MetPA showed significant changes (Holm P<0.05) only in TCA cycle between hemispheres after injury (Figure 3E). **MSEA showed significant (Holm P<0.05) fold enrichment in metabolite clusters related to transfer of acetyl groups into mitochondria and lipid metabolism (Figure 3F)**. Small metabolome differences between hemispheres in TBI emphasized the highly non-localized and diffuse nature of TBI-induced metabolic shifts throughout the injured brain.

3.3. Contralateral metabolic perturbations after TBI

To determine contralateral TBI impact, we compared contralateral hemisphere metabolic changes between sham and TBI. About 14% of metabolites showed a two-fold difference (Figure 4A) and as observed by the volcano plots, however,none of the targeted metabolites were significantly different between sham and TBI (Figure 4B). Multivariate analysis using PLS-DA (Figure 4C, D) showed a partial class separation with a positive accuracy value of the PLS-DA model (Accuracy=0.77, R^2 value=0.97, Q^2 value=0.42) (Figure S3B). Hierarchical clustering showed changes in fatty acids, amino acids/neurotransmitters with no significant effects on TCA cycle metabolites (Figure S3A**)**. These results confirm the diffuse nature of the lateralized TBI with broad metabolic shifts but relatively insignificant in effect across the contralateral hemisphere. MetPA and MSEA analyses also showed no significant impact on any metabolic pathways, as none of these were significantly impacted in the contralateral hemisphere between sham and TBI animals (Figure 4E, F).

3.4. Ipsilateral metabolic perturbations after TBI

Largest metabolomic differences were observed between the ipsilateral hemispheres of sham and TBI groups. About 33% of metabolites showed a two-fold difference (Figure 5A) and as observed by the volcano plots, 20% of the metabolites showed significant differences (corrected p<0.05) (Figure 5B). The 33% metabolites showing two fold changes (increase or decrease) are highlighted in **Table S1**. Multivariate PLS-DA (Figure 5C, D) showed distinct class separation with a high accuracy of the PLSDA model (Accuracy=0.88, R^2 value=0.98, Q^2 value=0.79) (Figure S4B). Hierarchical clustering and statistical threshold of 25 best hits

based on two-sample t-test showed differences in energy related metabolites, amino acids and fatty acid metabolites (Figure S4A). TBI had the highest impact on several metabolic pathways in the ipsilateral hemisphere as assessed by MetPA with significant changes (Holm $P<0.05$) related to pyruvate metabolism, TCA cycle, glyoxylate and dicarboxylate metabolism, vitamin B6 metabolism, nicotinate and nicotinamide metabolism, glycine, serine, and threonine metabolism and glycolysis (Figure 5E). **Furthermore, MSEA analysis also showed significant fold enrichment (Holm $P<0.05$) in metabolite clusters related to 25 metabolic pathways (Figure 5F). Some of these 25 metabolic pathways included betaine metabolism, lipid metabolism, glucose-alanine cycle, vitamin B6 metabolism, several amino acids metabolic pathways, TCA cycle, transfer of acetyl groups into mitochondria, malate-aspartate shuttle, oxidation of branched chain amino acids, glycolysis, urea cycle, phosphatidylcholine and phospholipid biosynthesis (Figure 5F)**. The results highlight the relatively more intense effect of the lateral fluid percussion TBI on the ipsilateral hemisphere impinging on several critical metabolic pathways.

3.5. Bilateral effect of TBI on sensorimotor behaviors

Sham and TBI animal groups underwent sensorimotor behavioral assessments using the whisker-stimulation induced motor reactivity (WSIMR) and forelimb usage tests. During ipsilateral whisker stimulation, TBI animals showed diminished motor reactivity compared to sham (Figure 6A). However, the intensity of diminished motor reactivity in response to contralateral whisker stimulation was relatively higher (Figure 6B). TBI animals also showed reduced usage of both forelimbs simultaneously to explore the cage surface compared to sham as indicated by reduced average forelimb usage scores (Figure 6C). In separate groups of sham and TBI animals, ipsilateral and contralateral forelimb usage was scored separately. Sham animals were observed to use both forelimbs simultaneously ~75–80% of the time, ~2% of the time they used only the ipsilateral forelimb and ~10–20% of the time they used only the contralateral forelimb to explore the surface (Figure 6D). However, TBI animals used both forelimbs simultaneously only ~45% of the time with increased usage of only the ipsilateral forelimb (~34%) or only the contralateral forelimb (~20%), indicating motor functional deficits across both hemispheres (Figure 6D). Further analysis after normalization to sham scores showed significant decreases in the simultaneous use of both forelimbs and significant increases in ipsilateral forelimb usage at 24, 48 and 72 hours after TBI (Figure 6E). Baseline behavioral assessments prior to luer-lock implantation for injury was not performed as the luer-lock needed lateral placement, which induced a behavioral asymmetry with reduced ipsilateral forelimb usage (Figure 6D). Hence TBI induced forelimb usage was normalized to sham (Figure 6D).

3.6. Neurodegeneration after TBI

Histological assessments were performed in a separate group of sham and TBI animals. Postmortem brains were fixed on the 8^{th} day post-TBI for histological assessment since maximum neuronal death occurred during the acute/subacute TBI window of 0–7 days in the current preclinical rat model of TBI (Lifshitz and Lisembee, 2011). A peri-lesional region distant from the fluid percussion impact area and significantly responsible for the sensorimotor behavioral functions was chosen to histologically determine neurodegeneration from secondary injury mechanisms. Histological analysis after cresyl violet staining of

coronal sections indicated no inter-hemispheric differences between ipsilateral and contralateral neuronal count ($S1_{BF}$ region) in the sham group (Figure 7A-D). However, differences were observed in the TBI group with a significant neuronal loss of 30% neuronal cell body counts in the ipsilateral $S1_{BF}$ (Figure 7A-D). Concentrations of NAA, a neuronal marker was determined across all experimental groups, which showed a significant decrease between sham and TBI in the ipsilateral hemisphere (**Figure 7E, and S4A**). Linear regression of NAA levels with histological neurodegeneration indicated a strong correlation (R^2=0.70) with decreases in NAA levels at 72 hours correlating with the extent of neurodegeneration 7 days after TBI (Figure 7F).

4. Discussion

We show that the mild to moderate intensity lateral fluid percussion TBI in early developmental age rats (P31) affected several brain metabolic pathways with relatively different impact across either hemisphere at 72 hours after injury. Sensorimotor behavioral deficits due to TBI corresponded with the severity of metabolic perturbation evidenced by a relatively stronger ipsilateral impact. Specifically, we report a continued depression in TCA cycle pathway even at 72hr post-TBI, accompanied by decreases in N-acetyl aspartate (NAA) in the ipsilateral hemisphere, indicating compromised neuronal integrity and neurodegeneration (Demougeot et al., 2001; Tallan et al., 1956). NAA decrease 3-days post TBI was an early predictor of subsequent neuronal loss as histochemically confirmed 7-days post TBI.

Brain energy metabolism is mainly oxidative followed by higher neurometabolic rates during development (2–9 years in humans) (Chugani et al., 1987). Developing brain also presents with proportionally higher cell numbers (Dobbing and Sands, 1973) and greater myelination (Paus et al., 2001; Reiss et al., 1996). Hence any stress, including TBI can affect the brain energy metabolism with potentially broad and sometimes detrimental outcomes. Within-subject analysis (ipsi vs contra) in sham group revealed significant perturbation in 2.5% of the targeted metabolites, indicating that the craniotomy followed by the luer-lock syringe hub implantation itself led to changes in a small group of metabolites (Figure 2). Majority of these metabolites were related to energy metabolism (Figure S5AE), alluding to the highly sensitive nature of brain energy metabolic response to stress during early development. MetPA and MSEA too revealed a significant impact of craniotomy on metabolic pathways related to amino acids, bile acid synthesis, pyruvate metabolism, glycolysis and malate-aspartate shuttle (Figure 2E and2F). Bile acids in the brain are transported across the blood-brain barrier from the circulation (Quinn et al., 2014) and few bile acids are also synthesized within the brain (Zheng et al., 2016), which act as neuroactive steroids (Schubring et al., 2012) and positively correlate with brain energy metabolism (Zheng et al., 2016). The results on craniotomy-induced surgical stress impacting local glycolytic energy metabolism, indicated the sensitive nature of developmental brain bioenergetics to local surgical stress.

Comparison of ipsi vs contra hemispheres within the TBI group showed significant differences in less than 2.5% of the targeted metabolites. Such a minimal univariate and multivariate difference between hemispheres (Figure 3A-D), indicated that TBI-induced

metabolomic perturbation may follow the highly diffuse patterns of injury with an inversely proportional impact with distance from the injury site. Pathway analysis showed significant changes in critical metabolite clusters related to the TCA cycle and fatty acid metabolism (Figure 3E, F), indicating that multivariate pathway-based analysis may provide sensitive biomarker clusters reporting on the intensity of metabolic impact after TBI. Furthermore, severity of sensorimotor deficits showed clear inter-hemispheric differences, which indicated that the possible origins of behavioral deficits might stem from the intensity of perturbation/dysfunction in critical metabolic pathways within the cellular populations that include TCA cycle and fatty acid metabolism. These pstream metabolic perturbations can lead to broad downstream consequences varying from axonal injury, synaptic circuit damage and collective excitability of neural circuits to influence the overall brain function and behavioral outcome after TBI (Park et al., 2008).

Between-group comparisons across sham and TBI in the contralateral hemisphere revealed the diffuse nature of the fluid percussion TBI with 11% of the metabolites showing a two-fold change (Figure 4A). Volcano plot (Figure 4B) and pathway analysis however, showed no significant perturbations in the contralateral hemisphere (Figure 4E, F). A smaller percentage of overall changes in the contralateral hemisphere of injured animals were obvious, given the attenuation of injury impact with distance from the injury epicenter. While the current study considered samples of whole cerebral hemispheres (without the cerebellum and brain stem), sample preparations from smaller regions of brain tissue may further improve the ability to distinguish spatially dependent metabolomic shifts across smaller regions of interest. NAA, a neuronal marker has been shown to decrease in brain regions undergoing acute or chronic neurodegeneration. Specifically TBI studies have characterized NAA as a translatable marker of neuronal viability in the injured brain, which correlated with the extent of neurodegeneration (Al-Samsam et al., 2000; Alessandri et al., 2000; Casey et al., 2008; Demougeot et al., 2001). We analyzed contralateral NAA levels and found no significant differences between sham and TBI (Figure 7E and Figure S3A), indicating that the smaller-scale metabolic changes were not sufficient to provoke significant loss of contralateral neuronal populations after TBI. These results were corroborated by the histological assessments 7 days after TBI, where no significant differences were observed in viable contralateral neuronal counts between sham and TBI (Figure 7D). Despite insignificant neural loss, altered contralateral neurovascular activity, neuronal functional connectivity and stimulus-induced brain circuit activation have been observed in the current model as determined by our earlier functional neuroimaging studies (Murugan et al., 2016; Parent et al., 2018). Independent studies on unilateral TBI models in rats with long term follow up (>8 months), also show progressive injury primarily in the ipsilateral brain (Hayward et al., 2010). Hence broad metabolomic perturbations, although relatively low in intensity can possibly lead to long-term modifications in brain function in distant regions from the injury epicenter and without any significant neurodegeneration. Future studies on early metabolomic effects after TBI in specific brain regions of interest along with long-term correlation with synaptic/axonal, microstructural and brain functional activity end points may better help determine the relationship between specific early metabolomic biomarker clusters and long-term pathological outcome.

Ipsilateral hemisphere between sham and TBI animal groups showed the highest change with 20% of the metabolites significantly changing (Figure 5B) along with a significant multivariate class separation (Figure 5 C, D). MetPA indicated a high impact of injury on 7 critical metabolic pathways (Figure 5E). Brain energy and mitochondrial respiration was significantly perturbed after injury as indicated by significant MetPA changes in TCA cycle, glycolysis, gluconeogenesis, pyruvate metabolism, vitamin B6 metabolism, nicotinate and nicotinamide metabolism. MSEA indicated significantly enriched metabolites related to mitochondrial fatty acid beta-oxidation of branched chain fatty acids, transfer of acetyl groups into mitochondria, lipid metabolism, phospholipid and phosphatidylcholine biosynthesis suggesting perturbations in fatty acid synthesis and degradation. Several amino acid metabolic pathways including glycine, serine, tryptophan, histidine, methionine, glutamate, aspartate, phenylalanine and tyrosine were also significantly affected after TBI. Betaine and vitamin B6 metabolism were significantly impacted by TBI, these metabolites play critical roles in one carbon metabolism meditated detoxification of cells through methylation (Locasale, 2013). Significant decreases in ipsilateral NAA levels (Figure S4A and Figure 7E) were observed accompanying these intense metabolic shifts along with significantly affected TCA cycle and glycolytic energy metabolism. Hence intense ipsilateral metabolic disturbances in multiple pathways, combined with depressed oxidative and glycolytic metabolism, may hasten secondary injury and neurodegenerative process following TBI (Figure 7D). These results concur with our earlier studies showing a large disruption in ipsilateral neural functional connectivity and cerebrovascular reactivity in the long term (2 months after TBI) (Murugan et al., 2016; Parent et al., 2018).

Secondary neuronal injury involves various downstream mechanisms in TBI pathology (Park et al., 2008). However central to neuronal injury is mitochondrial ion homeostatic and respiratory failure (Lifshitz and Lisembee, 2011; Prins et al., 2013; Robertson et al., 2007; Robertson et al., 2013; Robertson et al., 2006; Zadori et al., 2012). As brain energy metabolic depression can exacerbate excitotoxic neuronal death through failure of mitochondrial respiration (Pandya et al., 2007; Verweij et al., 2000), the current results where ipsilateral oxidative metabolic depression persisted even at 72 hours after TBI, suggests that neuronal death can be facilitated by metabolic depression in the acute/subacute stages after TBI during early development. Hence preservation of energy metabolism and mitochondrial function are crucial targets for improved outcomes in developmental TBI. Independent studies improving mitochondrial function using low dose treatments with mitochondrial uncouplers or metabolic facilitators have shown protection against TBI (Pandya et al., 2007; Talley Watts et al., 2014). Our recent studies targeting mitochondrial Ca^{2+} ion homeostasis in vivo by enhancing mitochondrial Ca^{2+} uptake and cycling through treatment with Kaempferol led to improved behavioral and brain functional outcomes in the current model of developmental TBI (Murugan et al., 2016).

Behavioral responses were measured in a non-blinded manner, which was a limitation. Furthermore, rapid brain removal and cryogenic freezing without any saline perfusion was prioritized in order to preserve high energy phosphate metabolites. Hence the circulating metabolite pool contributes to the reported brain metabolomic profiles and hence regional or lateralized neurovascular compromise induced by TBI may alter circulating metabolites and add to the overall TBI-induced metabolomic differences reported in this study. While the

present results represent the developmental TBI metabolome, future systematic studies in the adult, which differ in energy metabolism and substrate utilization (Netopilova et al., 1995), may help characterize age-dependent differences in the TBI metabolome.

Supplementary Material

Refer to Web version on PubMed Central for supplementary material.

Acknowledgements

This study was supported by funding from the New Jersey Commission for Brain injury research (**CBIR15IRG010; SK**), and National Institutes of Health (**R01NS097750; VS**). The authors thank Drs. Guoan Zhang and Zhe Cheng from the Proteomics and Metabolomics Core Facility, Weill Cornell Medicine, New York, NY for assistance in sample preparation and performance of the LC-MS measurements.

References

Al-Samsam RH, Alessandri B, and Bullock R (2000). Extracellular N-acetyl-aspartate as a biochemical marker of the severity of neuronal damage following experimental acute traumatic brain injury. J Neurotrauma 17, 31–39. [PubMed: 10674756]

Alessandri B, al-Samsam R, Corwin F, Fatouros P, Young HF, and Bullock RM (2000). Acute and late changes in N-acetyl-aspartate following diffuse axonal injury in rats: an MRI spectroscopy and microdialysis study. Neurological research 22, 705–712. [PubMed: 11091977]

Bahado-Singh RO, Graham SF, Han B et al. (2016a). Serum metabolomic markers for traumatic brain injury: a mouse model. Metabolomics 12:100.

Bahado-Singh RO, Graham SF, Turkoglu O et al. (2016b). Identification of candidate biomarkers of brain damage in a mouse model of closed head injury: a metabolomic pilot study. Metabolomics 12:42.

Casey PA, McKenna MC, Fiskum G, Saraswati M, and Robertson CL (2008). Early and sustained alterations in cerebral metabolism after traumatic brain injury in immature rats. J Neurotrauma 25, 603–614. [PubMed: 18454682]

Chugani HT, Phelps ME, and Mazziotta JC (1987). Positron emission tomography study of human brain functional development. Annals of neurology 22, 487–497. [PubMed: 3501693]

Daley M, Dekaban G, Bartha R et al. (2016). Metabolomics profiling of concussion in adolescent male hockey players: a novel diagnostic method. Metabolomics 12 :185.

Demougeot C, Garnier P, Mossiat C, Bertrand N, Giroud M, Beley A, and Marie C (2001). N-Acetylaspartate, a marker of both cellular dysfunction and neuronal loss: its relevance to studies of acute brain injury. J Neurochem 77, 408–415. [PubMed: 11299303]

Dobbing J, and Sands J (1973). Quantitative growth and development of human brain. Arch Dis Child 48, 757–767. [PubMed: 4796010]

Emmerich T, Abdullah L, Crynen G, Dretsch M, Evans J, Ait-Ghezala G, Reed J, Montague H, Chaytow H, Mathura V, et al. (2016). Plasma Lipidomic Profiling in a Military Population of Mild Traumatic Brain Injury and Post-Traumatic Stress Disorder with Apolipoprotein E varepsilon4-Dependent Effect. J Neurotrauma 33, 1331–1348. [PubMed: 26714394]

Emmerich T, Abdullah L, Ojo J, Mouzon B, Nguyen T, Laco GS, Crynen G, Evans JE, Reed J, Mullan M, et al. (2017). Mild TBI Results in a Long-Term Decrease in Circulating Phospholipids in a Mouse Model of Injury. Neuromolecular medicine 19, 122–135. [PubMed: 27540748]

Faul M, Xu L, Wald MM, and Coronado VG (2010). Traumatic brain injury in the United States: Emergency department visits, hospitalizations, and deaths. Centers for Disease Control and Prevention, National Center for Injury Prevention and Control, 891–904.

Glenn TC, Hirt D, Mendez G, McArthur DL, Sturtevant R, Wolahan S, Fazlollahi F, Ordon M, Bilgin-Freiert A, Ellingson B, et al. (2013). Metabolomic analysis of cerebral spinal fluid from patients with severe brain injury. Acta neurochirurgica Supplement 118, 115–119. [PubMed: 23564115]

Gupta A, Elgammal FS, Proddutur A, Shah S, and Santhakumar V (2012). Decrease in tonic inhibition contributes to increase in dentate semilunar granule cell excitability after brain injury. J Neurosci 32, 2523–2537. [PubMed: 22396425]

Hayward NM, Immonen R, Tuunanen PI, Ndode-Ekane XE, Grohn O, and Pitkanen A (2010). Association of chronic vascular changes with functional outcome after traumatic brain injury in rats. J Neurotrauma 27, 2203–2219. [PubMed: 20839948]

Lifshitz J, and Lisembee AM (2011). Neurodegeneration in the somatosensory cortex after experimental diffuse brain injury. Brain Struct Funct 217, 49–61. [PubMed: 21597967]

Locasale JW (2013). Serine, glycine and one-carbon units: cancer metabolism in full circle. Nature reviews Cancer 13, 572–583. [PubMed: 23822983]

Marino S, Zei E, Battaglini M, Vittori C, Buscalferri A, Bramanti P, Federico A, and De Stefano N (2007). Acute metabolic brain changes following traumatic brain injury and their relevance to clinical severity and outcome. Journal of neurology, neurosurgery, and psychiatry 78, 501–507.

McDonald JW, Silverstein FS, and Johnston MV (1988). Neurotoxicity of N-methyl-D-aspartate is markedly enhanced in developing rat central nervous system. Brain Res 459, 200–203. [PubMed: 3048538]

Mcdonald JW, Silverstein FS, and Johnston MV (1988b). Developmental Alteration in N-Methyl-D-Aspartate Receptor Channel Binding Characteristics and Its Relationship to Neurotoxicity in Immature Brain. Ann Neurol 24, 337-337.

Murugan M, Santhakumar V, and Kannurpatti S (2016). Facilitating mitochondrial calcium uptake improves activation-induced cerebral blood flow and behaviour after mTBI. Frontiers in Neuroscience.

Netopilova M, Drsata J, Kubova H, and Mares P (1995). Differences between immature and adult rats in brain glutamate decarboxylase inhibition by 3-mercaptopropionic acid. Epilepsy research 20, 179–184. [PubMed: 7796789]

Oresic M, Posti JP, Kamstrup-Nielsen MH, Takala RSK, Lingsma HF, Mattila I, Jantti S, Katila AJ, Carpenter KLH, Ala-Seppala H, et al. (2016). Human Serum Metabolites Associate With Severity and Patient Outcomes in Traumatic Brain Injury. EBioMedicine 12, 118–126. [PubMed: 27665050]

Pandya JD, Pauly JR, Nukala VN, Sebastian AH, Day KM, Korde AS, Maragos WF, Hall ED, and Sullivan PG (2007). Post-Injury Administration of Mitochondrial Uncouplers Increases Tissue Sparing and Improves Behavioral Outcome following Traumatic Brain Injury in Rodents. J Neurotrauma 24, 798–811. [PubMed: 17518535]

Parent M, Li Y, Santhakumar V, Hyder F, Sanganahalli BG, and Kannurpatti S (2018). Alterations of parenchymal microstructure, neuronal connectivity and cerebrovascular resistance at adolescence following mild to moderate traumatic brain injury in early development. J Neurotrauma.

Park E, Bell JD, and Baker AJ (2008). Traumatic brain injury: Can the consequences be stopped? Can Med Assoc J 178, 1163–1170. [PubMed: 18427091]

Pascual JM, Solivera J, Prieto R, Barrios L, Lopez-Larrubia P, Cerdan S, and Roda JM (2007). Time course of early metabolic changes following diffuse traumatic brain injury in rats as detected by (1)H NMR spectroscopy. J Neurotrauma 24, 944–959. [PubMed: 17600512]

Paus T, Collins DL, Evans AC, Leonard G, Pike B, and Zijdenbos A (2001). Maturation of white matter in the human brain: a review of magnetic resonance studies. Brain Res Bull 54, 255–266. [PubMed: 11287130]

Prins M, Greco T, Alexander D, and Giza CC (2013). The pathophysiology of traumatic brain injury at a glance. Disease models & mechanisms 6, 1307–1315. [PubMed: 24046353]

Quinn M, McMillin M, Galindo C, Frampton G, Pae HY, and DeMorrow S (2014). Bile acids permeabilize the blood brain barrier after bile duct ligation in rats via Rac1-dependent mechanisms. Digestive and liver disease:official journal of the Italian Society of Gastroenterology and the Italian Association for the Study of the Liver 46, 527–534.

Reiss AL, Abrams MT, Singer HS, Ross JL, and Denckla MB (1996). Brain development, gender and IQ in children. A volumetric imaging study. Brain 119 (Pt 5), 1763–1774. [PubMed: 8931596]

Robertson CL, Saraswati M, and Fiskum G (2007). Mitochondrial dysfunction early after traumatic brain injury in immature rats. J Neurochem 101, 1248–1257. [PubMed: 17403141]

Robertson CL, Saraswati M, Scafidi S, Fiskum G, Casey P, and McKenna MC (2013). Cerebral glucose metabolism in an immature rat model of pediatric traumatic brain injury. J Neurotrauma 30, 2066–2072. [PubMed: 24032394]

Robertson CL, Soane L, Siegel ZT, and Fiskum G (2006). The potential role of mitochondria in pediatric traumatic brain injury. Developmental neuroscience 28, 432–446. [PubMed: 16943666]

Schallert T, Fleming SM, Leasure JL, Tillerson JL, and Bland ST (2000). CNS plasticity and assessment of forelimb sensorimotor outcome in unilateral rat models of stroke, cortical ablation, parkinsonism and spinal cord injury. Neuropharmacology 39, 777–787. [PubMed: 10699444]

Schubring SR, Fleischer W, Lin JS, Haas HL, and Sergeeva OA (2012). The bile steroid chenodeoxycholate is a potent antagonist at NMDA and GABA(A) receptors. Neuroscience letters 506, 322–326. [PubMed: 22155097]

Sheth SA, Iavarone AT, Liebeskind DS, Won SJ, and Swanson RA (2015). Targeted Lipid Profiling Discovers Plasma Biomarkers of Acute Brain Injury. PLoS One 10, e0129735. [PubMed: 26076478]

Tallan HH, Moore S, and Stein WH (1956). N-Acetyl-L-aspartic acid in brain. J Biol Chem 219, 257–264. [PubMed: 13295277]

Talley Watts L, Long JA, Chemello J, Van Koughnet S, Fernandez A, Huang S, Shen Q, and Duong TQ (2014). Methylene blue is neuroprotective against mild traumatic brain injury. J Neurotrauma 31, 1063–1071. [PubMed: 24479842]

Tang L, Peng S, Bi Y, Shan P, and Hu X (2014). A new method combining LDA and PLS for dimension reduction. PLoS One 9, e96944. [PubMed: 24820185]

Thomas S, Prins ML, Samii M, and Hovda DA (2000). Cerebral metabolic response to traumatic brain injury sustained early in development: a 2-deoxy-D-glucose autoradiographic study. J Neurotrauma 17, 649–665. [PubMed: 10972242]

Verweij BH, Muizelaar JP, Vinas FC, Peterson PL, Xiong Y, and Lee CP (2000). Impaired cerebral mitochondrial function after traumatic brain injury in humans. J Neurosurg 93, 815–820. [PubMed: 11059663]

Viant MR, Lyeth BG, Miller MG, and Berman RF (2005). An NMR metabolomic investigation of early metabolic disturbances following traumatic brain injury in a mammalian model. NMR in biomedicine 18, 507–516. [PubMed: 16177961]

Xia J, Psychogios N, Young N, and Wishart DS (2009). MetaboAnalyst: a web server for metabolomic data analysis and interpretation. Nucleic acids research 37, W652–660. [PubMed: 19429898]

Xia J, Sinelnikov IV, Han B, and Wishart DS (2015). MetaboAnalyst 3.0--making metabolomics more meaningful. Nucleic acids research 43, W251–257. [PubMed: 25897128]

Xia J, and Wishart DS (2010a). MetPA: a web-based metabolomics tool for pathway analysis and visualization. Bioinformatics (Oxford, England) 26, 2342–2344.

Xia J, and Wishart DS (2010b). MSEA: a web-based tool to identify biologically meaningful patterns in quantitative metabolomic data. Nucleic acids research 38, W71–77. [PubMed: 20457745]

Yi L, Shi S, Wang Y, Huang W, Xia ZA, Xing Z, Peng W, and Wang Z (2016). Serum Metabolic Profiling Reveals Altered Metabolic Pathways in Patients with Post-traumatic Cognitive Impairments. Scientific reports 6, 21320. [PubMed: 26883691]

Yuan M, Breitkopf SB, Yang X, and Asara JM (2012). A positive/negative ion-switching, targeted mass spectrometry-based metabolomics platform for bodily fluids, cells, and fresh and fixed tissue.Nature protocols 7, 872–881. [PubMed: 22498707]

Zadori D, Klivenyi P, Szalardy L, Fulop F, Toldi J, and Vecsei L (2012). Mitochondrial disturbances, excitotoxicity, neuroinflammation and kynurenines: novel therapeutic strategies for neurodegenerative disorders. Journal of the neurological sciences 322, 187–191. [PubMed: 22749004]

Zheng F, Xia ZA, Zeng YF, Luo JK, Sun P, Cui HJ, Wang Y, Tang T, and Zhou YT (2017). Plasma metabolomics profiles in rats with acute traumatic brain injury. PLoS One 12, e0182025. [PubMed: 28771528]

Zheng X, Chen T, Zhao A, Wang X, Xie G, Huang F, Liu J, Zhao Q, Wang S, Wang C, et al. (2016). The Brain Metabolome of Male Rats across the Lifespan. Scientific reports 6, 24125. [PubMed: 27063670]

- Lateral fluid percussion TBI (mild/moderate intensity) is highly diffusive
- TBI affected bioenergetics, fatty acid and amino acid metabolism
- Pathway-specific biomarker clusters depict spatial variability of TBI
- Oxidative metabolism continues to be depressed at 72 hours post-TBI
- NAA levels predicted secondary neurodegeneration to a large extent.

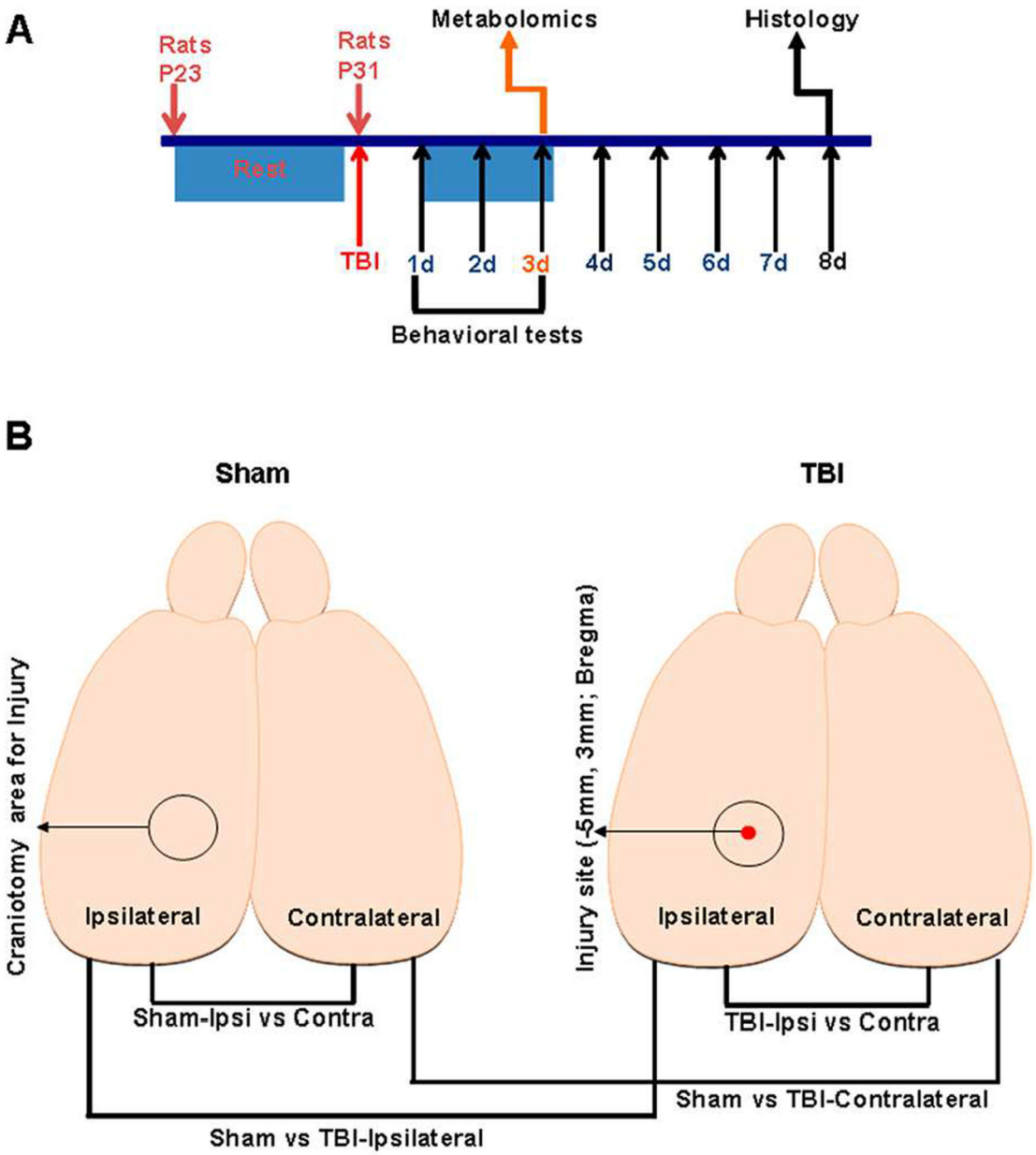

Figure 1.

A) Schematic of the experimental design and time line assessing effects of TBI on behavioral, metabolomic and histological outcomes. **B**) Schematic of the rat brain indicating the stereotaxic location of injury, craniotomy and experimental groups for statistical comparisons of metabolomic changes.

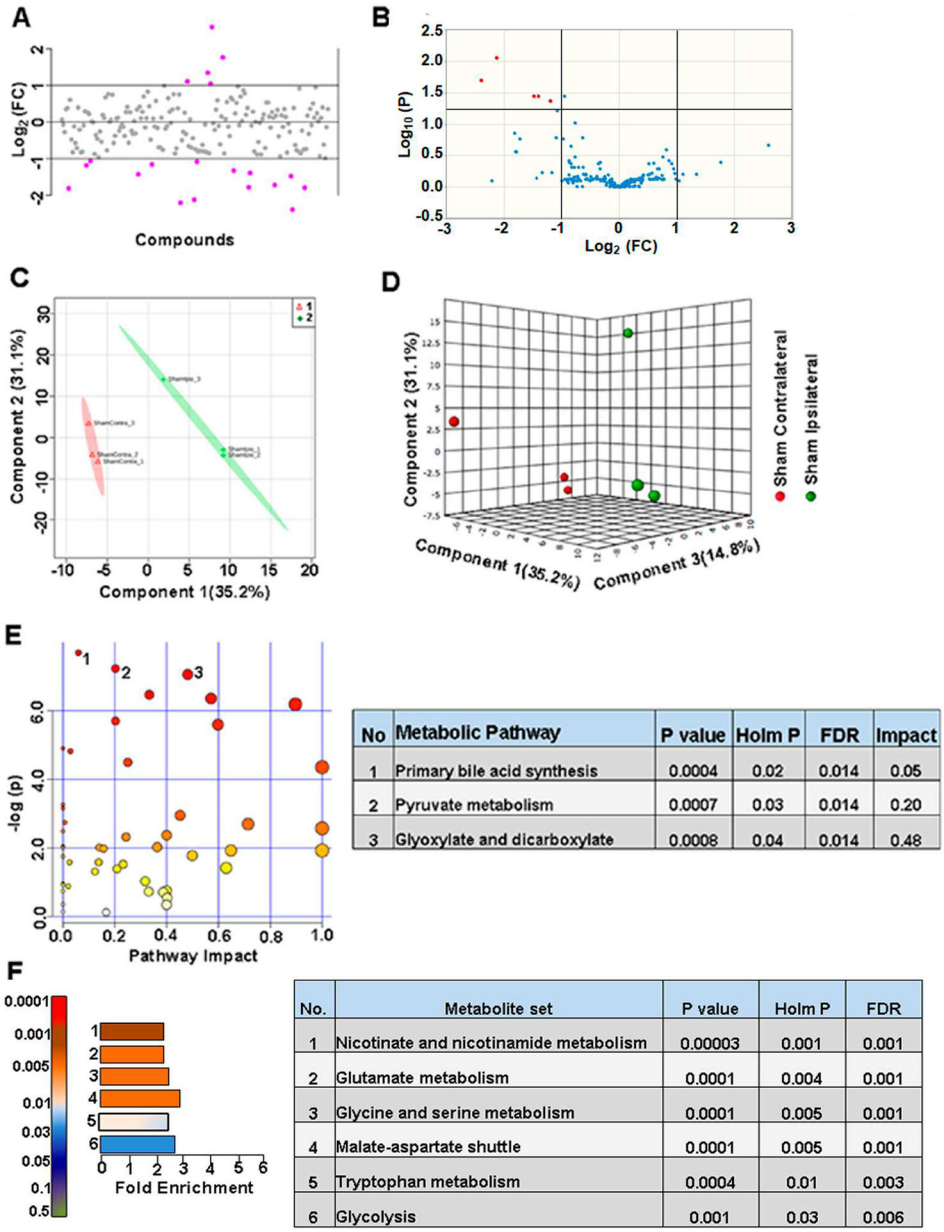

No	Metabolic Pathway	P value	Holm P	FDR	Impact
1	Primary bile acid synthesis	0.0004	0.02	0.014	0.05
2	Pyruvate metabolism	0.0007	0.03	0.014	0.20
3	Glyoxylate and dicarboxylate	0.0008	0.04	0.014	0.48

No.	Metabolite set	P value	Holm P	FDR
1	Nicotinate and nicotinamide metabolism	0.00003	0.001	0.001
2	Glutamate metabolism	0.0001	0.004	0.001
3	Glycine and serine metabolism	0.0001	0.005	0.001
4	Malate-aspartate shuttle	0.0001	0.005	0.001
5	Tryptophan metabolism	0.0004	0.01	0.003
6	Glycolysis	0.001	0.03	0.006

Figure 2. Craniotomy procedure perturbed about 9% of metabolites in sham animals

A) 19% of the metabolites showed a two-fold change in the ipsilateral compared to contralateral hemisphere. **B**) 2.5 % of the targeted metabolites were significantly different (corrected p<0.05; student's t-test). **C**) PLS-DA 2D scores plot, **D**) PLS-DA 3D scores plot showing partial class separation between sham contralateral (class 1) vs ipsilateral (class 2) hemispheres. **E**) MetPA. Left panel figure node colors are based on the p-value and node size on the pathway impact value. Table on the right shows significantly affected metabolic pathways. **F**) MSEA. Left panel figure y-axis indicates the metabolite set based on the holm p-value and x-axis, the fold enrichment. Table on the right shows affected pathways relevant to significantly enriched metabolite sets.

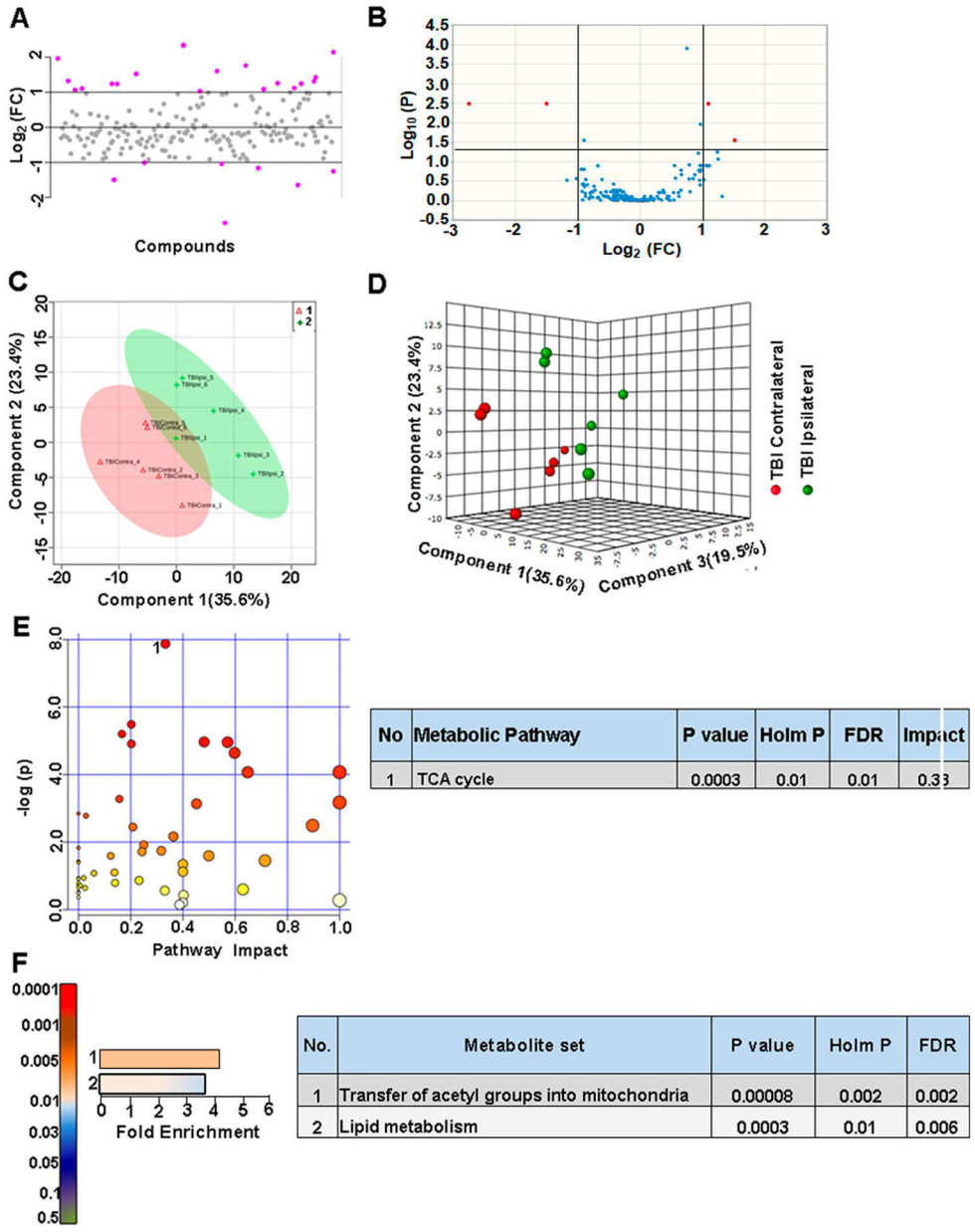

No	Metabolic Pathway	P value	Holm P	FDR	Impact
1	TCA cycle	0.0003	0.01	0.01	0.33

No.	Metabolite set	P value	Holm P	FDR
1	Transfer of acetyl groups into mitochondria	0.00008	0.002	0.002
2	Lipid metabolism	0.0003	0.01	0.006

Figure 3. Metabolic differences between ipsilateral and contralateral hemispheres in TBI animals

A) About 13% of the metabolites showed a two-fold change between ipsilateral and contralateral hemispheres in TBI animals. **B**) 2.5 % of the targeted metabolites were significantly different (corrected p<0.05; student's t-test). **C**) PLS-DA 2D scores plot, **D**) PLS-DA 3D scoresplot showing partial class separation between TBI contralateral (class 1) vs ipsilateral hemispheres (class 2). **E**) MetPA. Left panel figure node colors are based on the p-value and node size on the pathway impact value. Table on the right shows significantly affected metabolic pathways. **F**) MSEA. Left panel figure y-axis indicates the metabolite set based on the holm p-value and x-axis, the fold enrichment. Table on the right shows affected pathways relevant to significantly enriched metabolite sets.

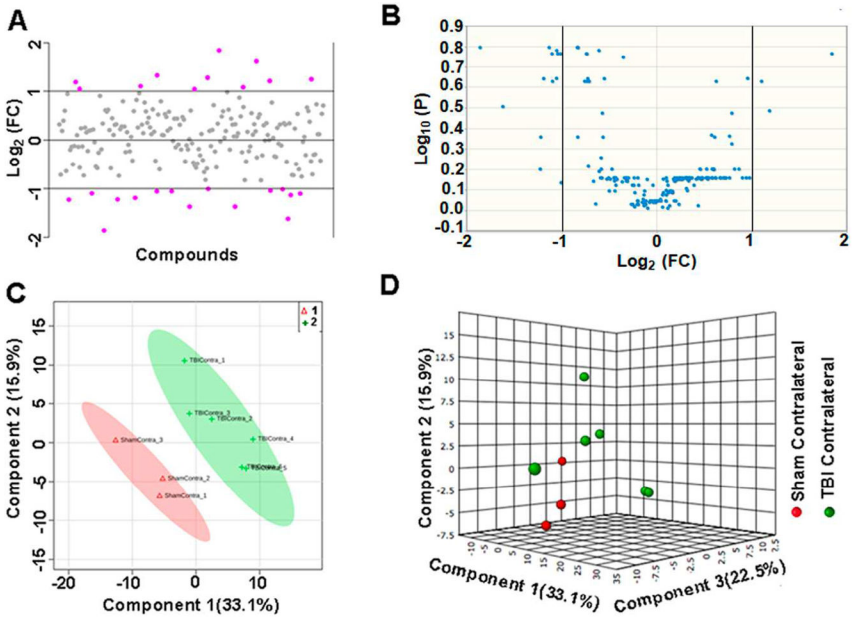

No	Metabolic Pathway	P value	Holm P	FDR	Impact
1	TCA cycle	0.005	0.25	0.16	0.33
2	Phenylalanine	0.013	0.61	0.16	0.64
3	Phenylalanine, tyrosine, and tryptophan	0.013	0.61	0.16	1

No.	Metabolite set	P value	Holm P	FDR
1	TCA cycle	0.003	0.1	0.1
2	Betaine metabolism	0.006	0.2	0.1
3	Lipid metabolism	0.009	0.3	0.1

Figure 4. TBI propagates to the contralateral hemisphere, inducing biochemical perturbations

A) About 14% of the metabolites showed a two-fold difference between sham vs TBI contralateral hemispheres. **B**) None of the targeted metabolites were significantly different. **C**) PLS-DA 2D scores plot, **D**) PLS-DA 3D scoresplot showing partial class separation between Sham contralateral (class 1) vs TBI contralateral hemispheres (class 2). **E**) MetPA. Left panel figure node colors are based on the p-value and node size on the pathway impact value. Table on the right shows significantly affected metabolic pathways. **F**) MSEA. Left panel figure y-axis indicates the metabolite set based on the holm p-value and x-axis, the fold enrichment. Table on the right shows affected pathways relevant to significantly enriched metabolite sets.

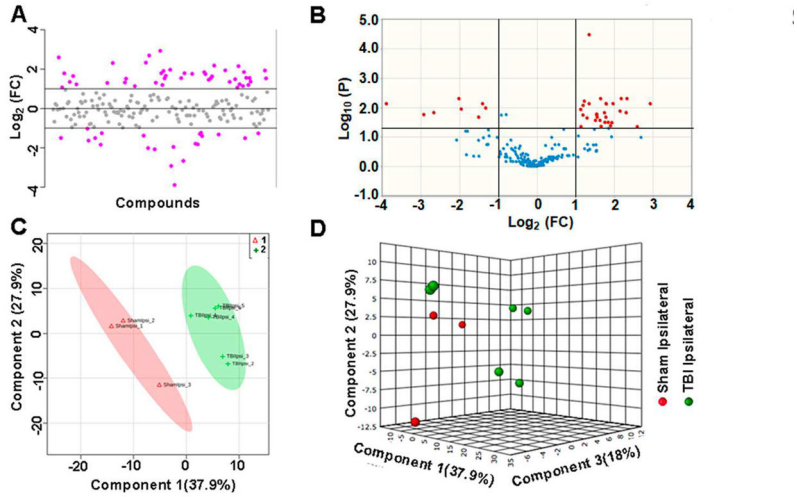

No	Metabolic Pathway	P value	Holm P	FDR	Impact
1	Pyruvate metabolism	0.00003	0.001	0.001	0.20
2	TCA cycle	0.00004	0.002	0.001	0.33
3	Glyoxylate and dicarboxylate	0.0001	0.007	0.002	0.48
4	Vitamin B6 metabolism	0.0002	0.01	0.002	0.16
5	Nicotinate and nicotinamide	0.0004	0.01	0.003	0.55
6	Glycine, serine and threonine	0.0005	0.02	0.004	0.57
7	Glycolysis or Gluconeogenesis	0.0007	0.03	0.004	0.20

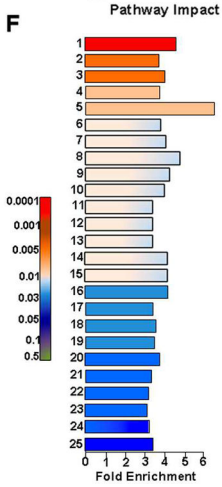

No.	Metabolite set	P value	Holm P	FDR
1	Betaine metabolism	0.000008	0.0002	0.0002
2	Lipid metabolism	0.0001	0.004	0.001
3	Glucose-alanine cycle	0.0001	0.004	0.001
4	Glycine and serine metabolism	0.0002	0.008	0.001
5	Vitamin B6 metabolism	0.0003	0.009	0.001
6	Tryptophan metabolism	0.0003	0.01	0.001
7	Transfer of acetyl groups into mitochondria	0.0004	0.01	0.001
8	Oxidative and mitochondrial metabolism	0.0004	0.01	0.001
9	Citric acid cycle	0.0005	0.01	0.001
10	Malate-Aspartate shuttle	0.0005	0.01	0.001
11	Histidine metabolism	0.0007	0.01	0.002
12	Oxidation of branched chain fatty acids	0.0008	0.01	0.002
13	Methionine metabolism	0.0008	0.01	0.002
14	Phenylalanine and tyrosine metabolism	0.0008	0.01	0.002
15	Nicotinate and nicotinamide metabolism	0.0009	0.01	0.002
16	Pyruvate metabolism	0.001	0.02	0.002
17	Glutamate metabolism	0.001	0.02	0.002
18	Glycolysis	0.001	0.02	0.002
19	Urea cycle	0.001	0.02	0.003
20	Gluconeogenesis	0.002	0.03	0.003
21	Tyrosine metabolism	0.002	0.03	0.003
22	Ammonia recycling	0.002	0.03	0.003
23	Aspartate metabolism	0.002	0.03	0.004
24	Phosphatidylcholine biosynthesis	0.003	0.04	0.005
25	Phospholipid biosynthesis	0.005	0.05	0.007

Figure 5. Intense ipsilateral metabolic perturbations after TBI

A) Injury on the ipsilateral hemisphere showed two-fold change in about 32% of the targeted metabolites. **B**) 20% of the targeted metabolites were significantly different between the ipsilateral hemispheres of sham vs TBI (corrected $p<0.05$; student's t-test). **C**) PLS-DA 2D scores plot, **D**) PLSDA 3D scores plot showing distinct class separation between Sham ipsilateral (class 1) vs TBI ipsilateral hemispheres (class 2). **E**) MetPA. Left panel figure node colors are based on the p-value and node size on the pathway impact value. Table on the right shows significantly affected metabolic pathways. **F**) MSEA. Left panel figure y-axis indicates the metabolite set based on the holm p-value and x-axis, the fold enrichment. Table on the right shows affected pathways relevant to significantly enriched metabolite sets.

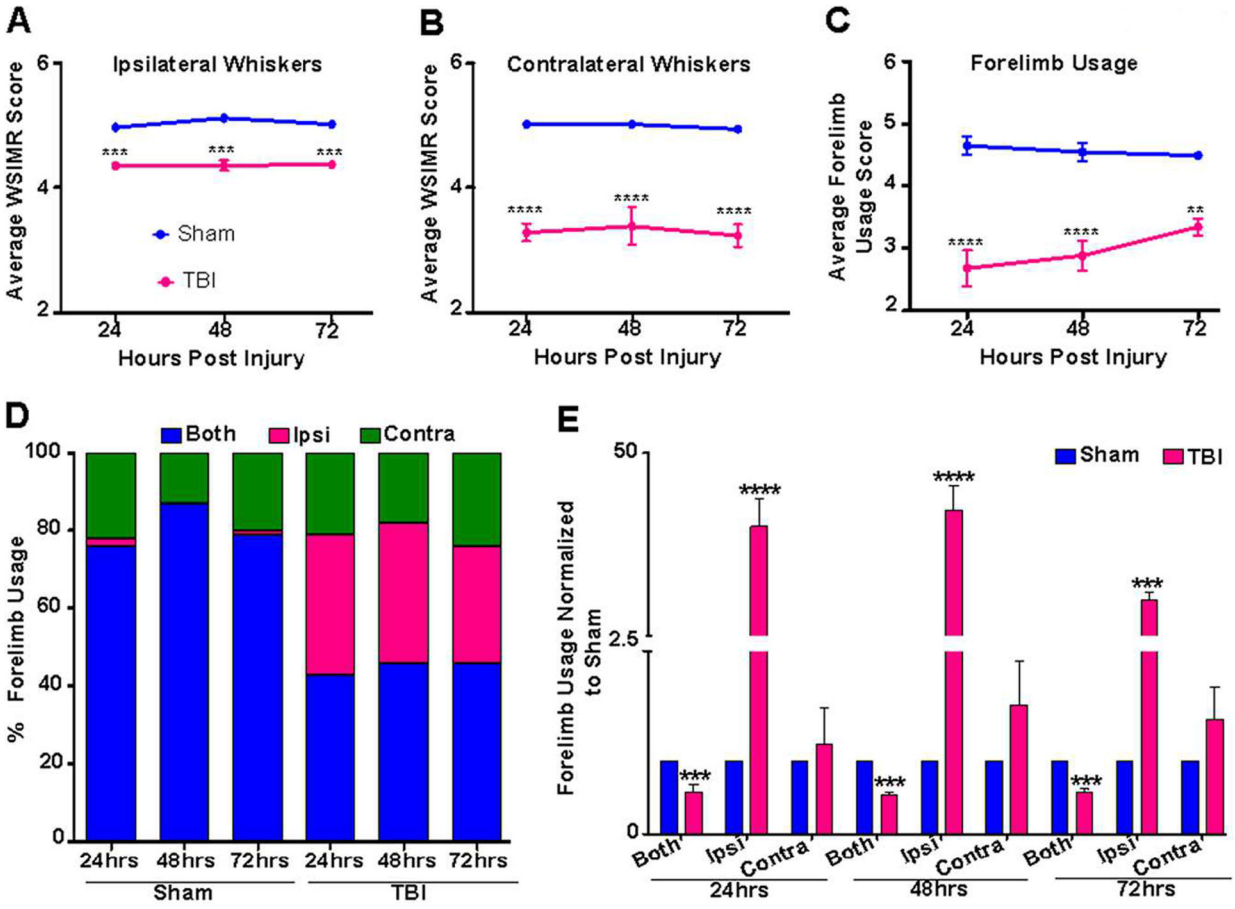

Figure 6. Early stage sensorimotor behavioral asymmetry after TBI

A) TBI animals (pink) exhibited reduced WSIMR in response to ipsilateral whisker stimulation compared to sham animals (blue). **B**) Intensity of diminished motor activity in response to contralateral whisker stimulation was much higher compared to the ipsilateral activity in TBI animals. **C**) Forelimb debilitation test in TBI animals showed deficient use of both forelimbs (pink) compared to sham animals (blue). **D)** Percentage forelimb usage in sham and TBI animals at 24, 48, and 72 hours after injury. TBI animals used both forelimbs simultaneously (blue) ~45% of the time, with an increased usage of only ipsi forelimb (pink) (~34%) or only contra forelimb (green) (~20%) when compared to sham animals, indicating profound motor functional deficits on both brain hemispheres after TBI. **E)** Percentage forelimb usage in TBI animals normalized to sham. TBI animals decreased the simultaneous usage of both forelimbs with a significant increase in ipsilateral forelimb usage at 24, 48 and 72 hours after injury compared to sham. Significantly different; ***p<0.001; **p<0.01; two-way RM ANOVA. Error bars, SEM.

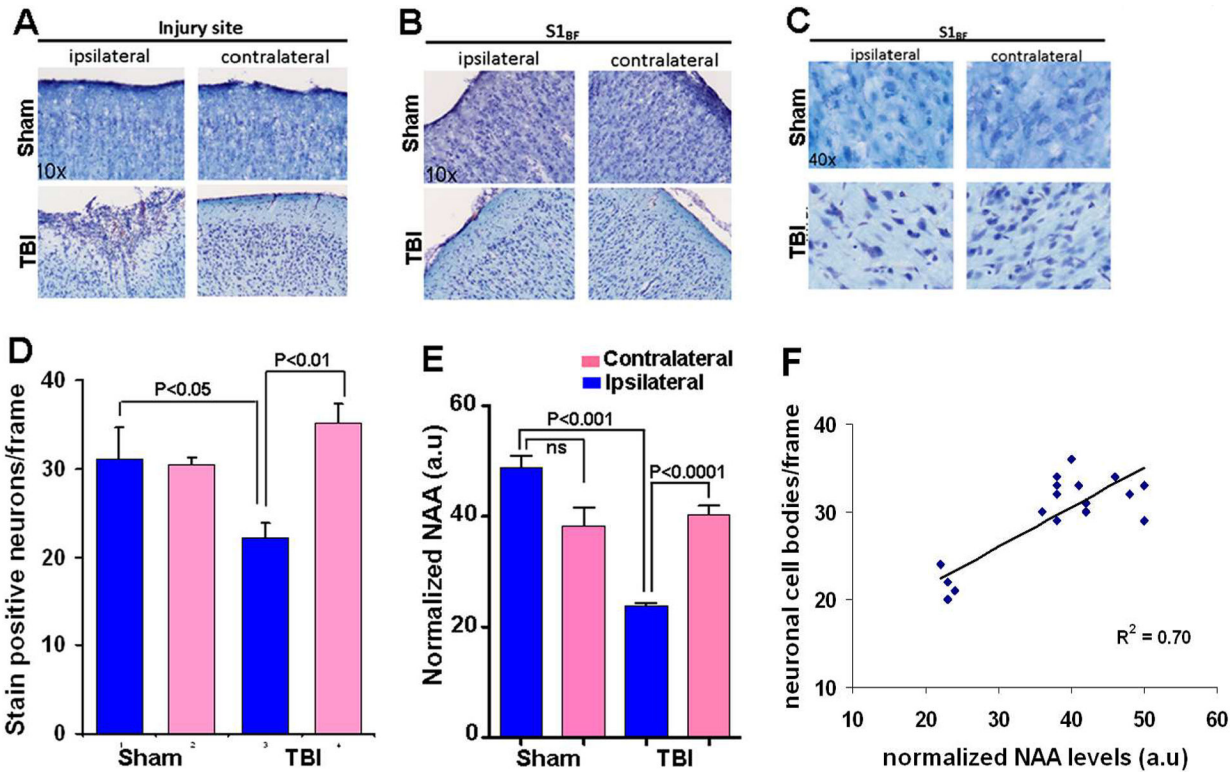

Figure 7. Cresyl violet stained post fixed and cryosectioned brain slices (coronal plane) at the 8th day after TBI

Representative coronal sections at **A**) Injury site and **B)** Whisker barrel cortex ($S1_{BF}$).**C**) $S1_{BF}$ region at higher magnification, (representational frame used for neuronal counting). **D)** Number of stain positive neuronal cell bodies counted per frame from different layers of the $S1_{BF}$ region. Data represent mean ± SD value of 4 sham and 5 TBI animals. Comparisons between ipsilateral and contralateral neuronal counts indicated significant neuronal loss in the ipsilateral cortex of TBI animals. **E)** NAA levels normalized to global mean. TBI ipsilateral hemisphere showed reduced levels of NAA compared to sham ipsilateral and TBI contralateral hemispheres. Significant differences tested by ANOVA post-hoc Tukey's HSD test or two-way ANOVA. **F)** Linear regression of neuronal counts/frame and normalized NAA levels from sham and TBI animals in both hemispheres (9 animals).